ENHANCED NONINVASIVE IMAGING SYSTEM FOR DISPERSIVE HIGHLY COHERENT SPACE

Muhammad Naveed Tabassum, Ibrahim Elshafiey, Mubashir Alam

Department of Electrical Engineering, King Saud University, Riyadh, Kingdom of Saudi Arabia

ABSTRACT

A new noninvasive nearfield electromagnetic imaging (EMI) system for highly coherent and compressively sensed (CS) data at only few sensing positions is presented in this paper. Principal component analysis (PCA) in combination with spatial CS and background subtraction is implemented for the enhanced imaging of highly dispersive and coherent target space. The proposed imaging system is applied by forming an incoherent dictionary, which is later tested and validated for head imaging of single and multiple brain tumor targets using CS based sparse recovery. The head imaging model containing the tumor with an applicator antenna array around it is designed using CST Microwave Studio. Consequently, enhanced imaging results reveal the potential of the developed imaging system.

***Index Terms*—**Principal component analysis, nearfield imaging, electromagnetic imaging, head imaging, compressed sensing, sparse recovery

1. INTRODUCTION

Noninvasive electromagnetic imaging (EMI) for targets in the nearfield using radio and microwave frequencies is an attractive research area. Therefore, it has various industrial, security and biomedical applications such as: underground object detection, nondestructive testing, security inspection and medical diagnostic and imaging [1-3]. Moreover, these all applications benefit from the penetration ability of EM signal pulses of radio and microwave frequencies. Indeed, EMI using radio and microwave frequencies provides simple and inexpensive systems by using non-ionizing EM fields.

The main objective of the work presented in this paper is to propose a new noninvasive nearfield EMI system for highly coherent, compressively sensed (CS) data at only few sensing positions. The proposed system is applied and tested here for the enhancement of head imaging. As, the contrast in electrical properties for cancerous and healthy tissues has been used in breast tumor imaging [1, 2]. However, head imaging has proven to be more challenging [3]. This is due to the geometrical complexity of the head and the higher dispersive material properties of the brain tissues compared to that of breast tissues. Therefore, resulting in higher attenuations for the propagation of EM signal pulses. Furthermore, the received scattered time-domain signals at the sensing positions are extremely weak due to higher attenuations incurred. Thus, these received signals for different possible tumor target locations have very small difference. This results in a dictionary formation with maximum spatial coherence making it difficult to differentiate between different possible tumor locations.

Moreover, wideband transmitted EM signals results in large amounts of scattered data for materials with higher dispersive properties such as: brain, grey matter and cerebrospinal fluid (CSF). This results in large amounts of data to be collected at a large number of sensing positions. This problem of complex and highly coherent data collection needs to be addressed. Advance signal processing is thus necessary to extract useful information from highly coherent and compressively sensed data at few sensors.

In this paper, principal component analysis (PCA) in addition to spatial compressed sensing (CS) and background subtraction is implemented to overcome above mentioned problems [4, 5]. Consequently, overall imaging system herein consists of an applicator antenna array, head imaging model, data collection setup and a post processing setup which is implemented to process and invert the collected data to have enhanced imaging of highly dispersive and spatially coherent target space.

This paper is presented as follows. The head imaging model for recording of receiving signals for tumor anomaly by an applicator antenna array is described in Section 2. Compressively sensed incoherent dictionary is formed in Section 3, which is required for sparse imaging using CS in Section 4. The enhanced imaging results are presented in Section 5 with conclusions in Section 6.

2. HEAD IMAGING MODEL

The head imaging model is designed using advanced computational and electromagnetic (EM) simulations in CST Microwave Studio (MWS). The head arrangement consists of four layered cylindrical shapes. In this, the first cylinder

This work was supported by NSTIP strategic technologies program number (10-ELE996-02) in the Kingdom of Saudi Arabia. The research is also supported by the College of Engineering Research Center and the Deanship of Scientific Research at King Saud University.

represents average brain tissue with a radius of *80* millimeter. Likewise, second, third and fourth cylinders represent the grey matter, cerebrospinal fluid (CSF) and skull and have a radius of *84*, *89* and *94* millimeters respectively as shown in Fig. 1. Moreover, this head configuration contains the tumor anomaly inside it as shown in Fig. 1. Henceforth, the dispersive material properties are assigned to the tumor according to the contrast used in [6], which is 2:1 relative to the surrounding brain tissue in the electrical conductivity and 1.6:1 in the relative permittivity.

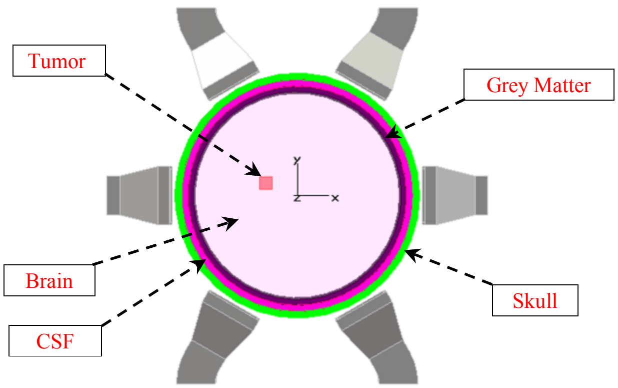

Fig. 1. Head imaging model with tumor and antenna array.

Horn antenna is used as elements for the applicator antenna array as shown in Fig. 1. Furthermore, a wideband EM signal of the Gaussian sine pulse is used for the transmission of EM energy by the excitation of applicator antenna array elements. Accordingly, the operational range of wideband frequencies is selected from 300-3000 megahertz, as this gives a good compromise on resolution of the reconstructed image, penetration for EM signals and the antenna size. Consequently, the input signal pulse covering the operational frequency range is shown in Fig. 2a.

The materials used herein like brain tissue, grey matter, cerebrospinal fluid (CSF) and skull are all dispersive. Thus, these materials need to fit a certain dispersion model to have wideband material behavior for the operating frequency range. Therefore, an n^{th} order dispersion-fitting model is applied herein. The sample points assigned according to the values reported in the literature [7] and their related fitting curves are shown in Fig. 2b and 2c for brain tissue. Similarly, other materials are fitted to have dispersion-fitting curves for operating wideband frequency range.

The received time-domain signals are collected compressively at only six sensing positions in the space. Therefore, the applicator antenna array consists of only six elements as shown in Fig. 1.

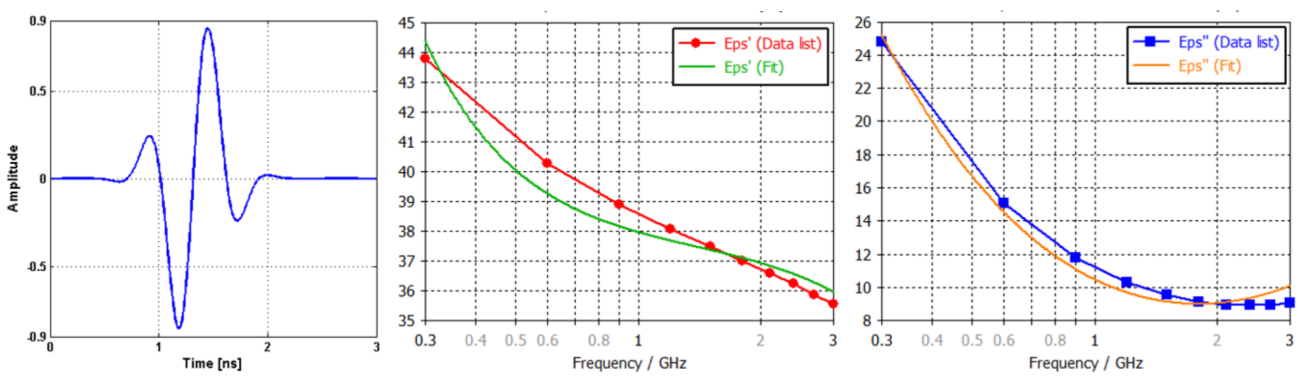

(a) (b) (c)

Fig. 2. (a) Input time-domain signal for excitation of array elements and (b) and (c) dispersion-fitting curves for brain tissue.

A sample of the received time-domain signal collected at an element of the applicator antenna array is shown in Fig. 3a. Furthermore, the received time-domain signals at each element can be recognized by four parts [8] as indicated in Fig. 3a: the coupled signal from elements of the applicator antenna array, the reflected signal from skull, CSF, grey matter and brain tissue layers, the tumor reflections and the clutter.

3. INCOHERENT DICTIONARY FORMATION

3.1. Background Subtraction

The proposed Imaging system treats the imaging problem here as a dictionary selection problem. Therefore, the dictionary is formed by discretizing the target space. Thus, the discretization results in a finite set of possible tumor locations $B = \{\beta_1, \beta_2, \ldots.. , \beta_N\}$ where N is the target space resolution and each β_j is a 3D location with cylindrical coordinates $[r_j, \theta_j, z_j]$ but here z_j is made fix at origin.

The received time-domain signal at each element of the antenna array as one given in Fig. 3a is preprocessed for the background and other reflections subtraction. It can be seen that due to the large attenuations presented by the layers with higher dispersive material properties in head model, the resulting signal in Fig. 3b after subtraction is extremely weak having very small magnitudes. However, still there are few samples around 25% of the total samples, which are useful for the extraction of information about tumor presence.

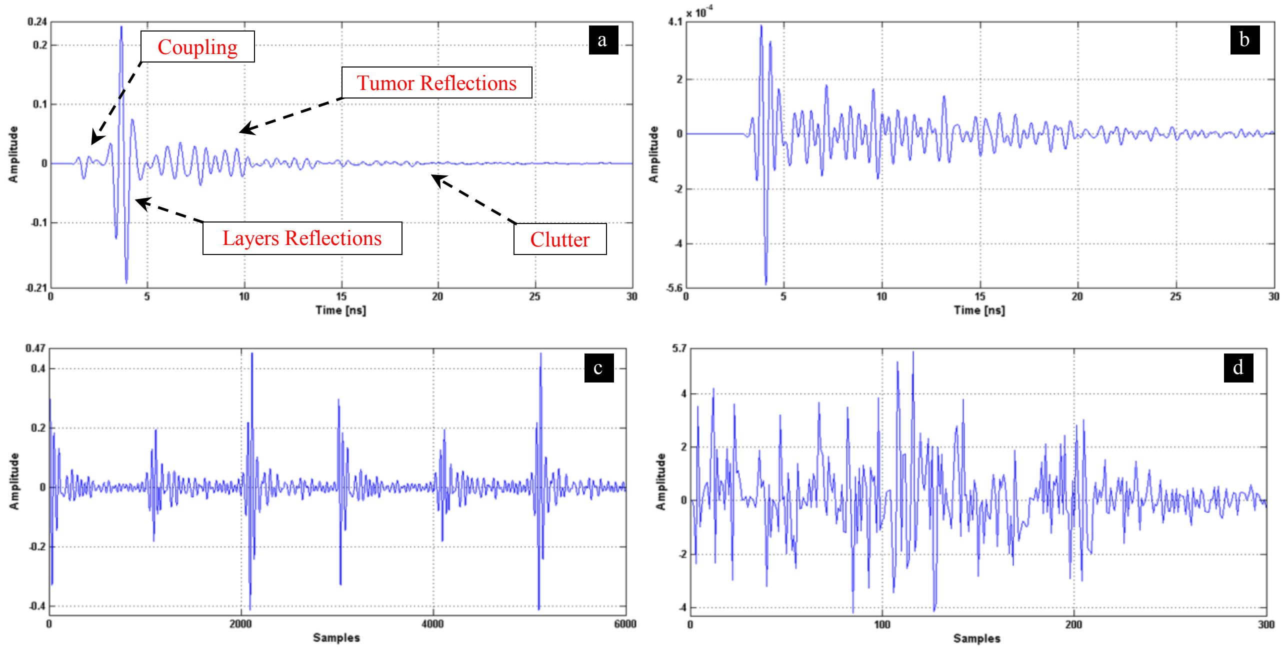

Fig. 3. Received scattered time-domain signal at an array element (a) before and (b) after background and other reflections subtraction. The difference signal for two random observations in dictionary (c) before and (d) after PCA implementation.

Therefore, considering the received time-domain signal to be described by *λ-samples* for each array element, only the useful samples are selected for the analysis resulting in signal with *ρ-samples* (ρ=0.25λ) for each element. This preprocessing is repeated for all L elements to synthesize a single observation signal, described by P samples as:

$$P = [\rho_1, \rho_2, \ldots, \rho_L]^T, \qquad \text{where T=Transpose} \qquad (1)$$

The entries in the dictionary are formed by implementing Eq. 1 for only few of the total N discrete possible tumor locations, resulting in spatial compressed sensing. These few locations were selected randomly from the target space. Afterwards, the linear interpolation is implemented to fit the data for the rest of the target space, resulting in full dictionary $\Phi \in \mathbb{R}^{P\times N}$ with N observation signals for full target space each described by P samples.

3.2. Principal Component Analysis

The signal observations in the resulting dictionary are highly coherent and have insufficient difference to be differentiable as shown in Fig. 3c for a random pair of observations. Therefore, PCA is employed, which analyzes the inter-correlated data with N observations each described by several samples [9] as herein by P. Its objective is to extract the most significant information from the data and to express this information as a set of new M orthogonal samples called principal components, which contain the maximum variance of the data [9]. Therefore, first of all columns of $\Phi^T \in \mathbb{R}^{N\times P}$ were centered so that the mean of each column is equal to zero [9]. Afterwards, covariance matrix is computed and the eigenvectors and eigenvalues were found using singular value decomposition (SVD). Eigenvalue for corresponding eigenvector represents the amount of variance that the given eigenvector accounts for [9]. So, the eigenvectors are sorted in decreasing order of the eigenvalues giving eigenvectors in order of significance. The first M eigenvectors from B are selected which accounts for *90%* of the variation.

The dictionary is whitened firstly by making the rows of $\Phi^T \in \mathbb{R}^{N\times P}$ uncorrelated by projecting the dataset onto the eigenvectors which results in dataset rotation. Secondly, the dataset is normalized to have a unit variance for all components by simply dividing each component by the square root of its eigenvalue. Collectively, all of the above transformations of the original P samples to the M principal components are given by Eq. 2 as:

$$A = TU\Phi \qquad (2)$$

Where $T \in \mathbb{R}^{M\times M}$ is the whitening transformation matrix and rows of matrix $U \in \mathbb{R}^{M\times P}$ are first M eigenvectors. This results in final dictionary $A \in \mathbb{R}^{M\times N}$, which will be used for imaging using CS based sparse recovery. Accordingly, signal observations in the resultant dictionary are now less coherent and have sufficient difference to be differentiable as shown in Fig. 3d for a same random pair of observations.

4. IMAGING USING COMPRESSED SENSING

Compressed sensing (CS) theory states that sparse signals and images can be reconstructed from far fewer samples than those by using traditional Shannon-Nyquist rates [10, 11]. The important principles underlying CS are *sparsity* and *incoherence* [10]. The target space to be reconstructed here is sparse and the incoherent dictionary $A \in \mathbb{R}^{M\times N}$ with $M<<N$ has been formed by employing PCA, making the CS based sparse recovery applicable.

The compressed sensing theory proves that for a given dictionary $A \in \mathbb{R}^{M\times N}$, the CS based sparse recovery algorithm can reconstruct the *K-sparse* target space $x \in \mathbb{R}^{N\times 1}$, which maps the tumor distribution from a relatively smaller number of measurements $M<<N$ as a vector $y \in \mathbb{R}^{M\times 1}$ by:

$$y = Ax + \xi \tag{3}$$

Where $\xi \in \mathbb{R}^{M\times 1}$ represents the amount of noise. Although the system is ill-posed and underdetermined but due to the prior information of signal sparsity, $x \in \mathbb{R}^{N\times 1}$ can be perfectly reconstructed with high probability via properly designed recovery algorithm. There are various CS based sparse recovery algorithms available in the literature which can be used. Among them the greedy search algorithm receives significant interest. The compressive sampling matching pursuit (CoSaMP) algorithm is implemented here for the imaging using CS [11] and compared with orthogonal matching pursuit (OMP) [12].

5. ENHANCED IMAGING RESULTS

The head imaging model is simulated for the detection of single tumor of complex shape and multiple tumors of different shapes and sizes to test and validate the proposed imaging system. The tumor under test is a combination of the 1 millimeter point targets. Therefore, the measurements vector y is a superposition of the observation signals for them as it is assumed here that the point targets at discrete spatial locations do not interact making superposition valid. The acquired measurements vector y is preprocessed to have an M number of samples. Enhanced imaging results for single tumor of complex shape (Fig. 6a) and for multiple tumors of different shapes and sizes at different locations (Fig. 6d) are reconstructed using the CoSaMP reconstruction algorithm (Fig. 6c and 6f) and are compared with those using the OMP reconstruction algorithm (Fig. 6b and 6e).

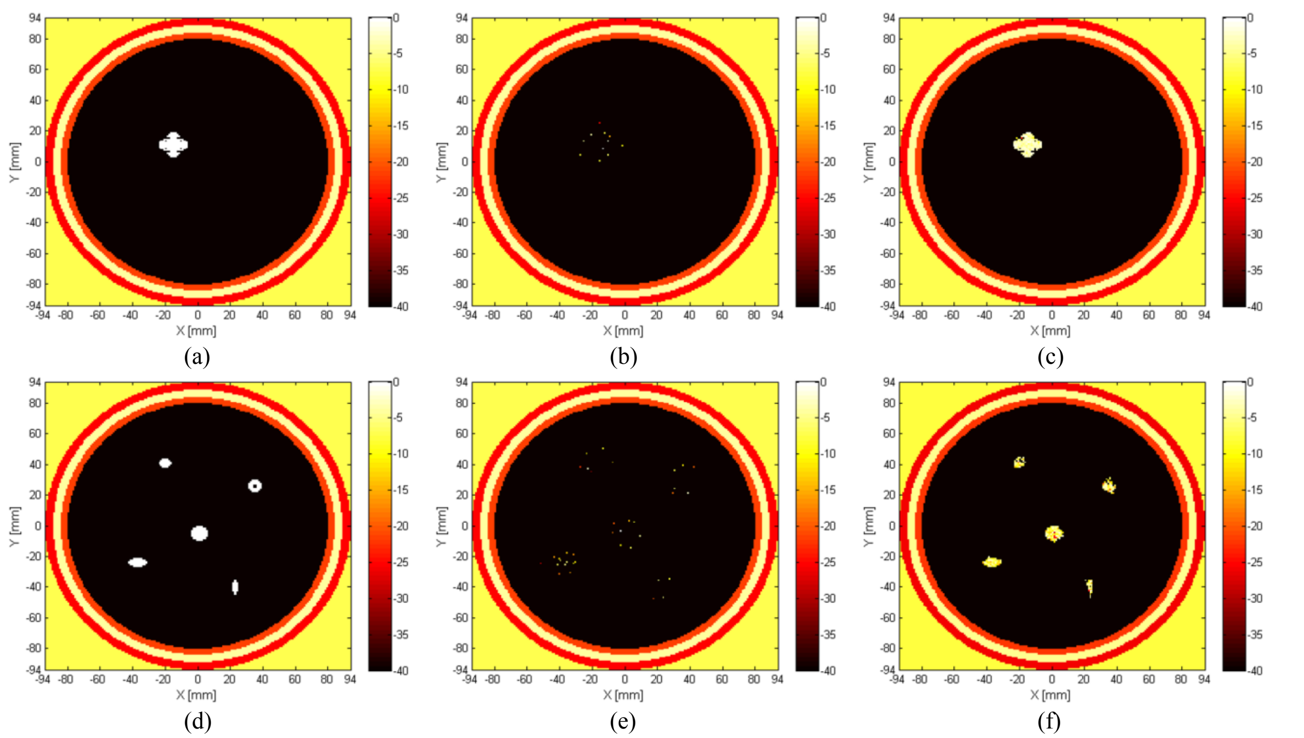

Fig. 4. Target space (a) with single brain tumor of complex shape and (d) with multiple brain tumors of different shapes and sizes at different locations. The imaging results for target space (b) and (e) using OMP and (c) and (f) using CoSaMP.

6. CONCLUSIONS

A new noninvasive nearfield EMI system for highly coherent, compressively sensed (CS) dictionary at only few sensing positions is proposed and applied to the head imaging of brain tumors for testing. The simulation for the head imaging model is conducted with tumor anomaly and applicator antenna array in CST MWS. The incoherent dictionary is formed by implementing PCA in combination with spatial CS and background and other reflections subtraction. Thus, the resulting dictionary with sufficient difference and less spatial coherence for signal observations is tested for head imaging of brain tumor targets. The enhanced imaging results with high-resolution shows the validity of proposed imaging system of incoherent dictionary formation and later testing it by CS based sparse imaging.

7. REFERENCES

[1] N. K. Nikolova, "Microwave imaging for breast cancer," *IEEE Microwave Magazine,* vol. 12, pp. 78-94, 2011.

[2] T. M. Grzegorczyk, P. M. Meaney, P. A. Kaufman, R. M. di Florio-Alexander, and K. D. Paulsen, "Fast 3-D Tomographic Microwave Imaging for Breast Cancer Detection," *IEEE Transactions on Medical Imaging,* vol. 31, pp. 1584-1592, 2012.

[3] B. J. Mohammed, A. M. Abbosh, S. Mustafa, and D. Ireland, "Microwave System for Head Imaging," *IEEE Transactions on Instrumentation and Measurement,* vol. 63, pp. 117-123, 2014.

[4] M. N. Tabassum, I. Elshafiey, and M. Alam, "Compressed Sensing Based Nearfield Electromagnetic Imaging," in *Proceedings of 4th IEEE International Conference on Control System, Computing and Engineering (ICCSCE)*, Penang, Malaysia, November, 2014.

[5] M. N. Tabassum, I. Elshafiey, and M. Alam, "Innovative Nearfield Electromagnetic Imaging System," in *Proceedings of IEEE International Conference on Smart Instrumentation, Measurement and Applications (ICSIMA)*, Kuala Lumpur, Malaysia, November, 2014.

[6] S. M. Yacoob and N. S. Hassan, "FDTD analysis of a noninvasive hyperthermia system for brain tumors," *Biomedical engineering online,* vol. 11, p. 47, 2012.

[7] C. Gabriel, "Compilation of the Dielectric Properties of Body Tissues at RF and Microwave Frequencies," U.S. Air Force Report AFOSR-TR-96, http://transition.fcc.gov/oet/rfsafety/dielectric.html.

[8] Z. Haoyu, A. O. El-Rayis, N. Haridas, N. H. Noordin, A. T. Erdogan, and T. Arslan, "A smart antenna array for brain cancer detection," in *Antennas and Propagation Conference (LAPC), 2011 Loughborough*, 2011, pp. 1-4.

[9] H. Abdi and L. J. Williams, "Principal component analysis," *Wiley Interdisciplinary Reviews: Computational Statistics,* vol. 2, pp. 433-459, 2010.

[10] E. J. Candès and M. B. Wakin, "An introduction to compressive sampling," *IEEE Signal Processing Magazine,* vol. 25, pp. 21-30, 2008.

[11] D. Needell and J. A. Tropp, "CoSaMP: Iterative signal recovery from incomplete and inaccurate samples," *Applied and Computational Harmonic Analysis,* vol. 26, pp. 301-321, 2009.

[12] J. A. Tropp and A. C. Gilbert, "Signal recovery from random measurements via orthogonal matching pursuit," *IEEE Transactions on Information Theory,* vol. 53, pp. 4655-4666, 2007.